Investigation of cross-field electron transport in a 100-W class Hall Thruster using a full particle-in-cell simulation

IEPC-2019-718

Presented at the 36th International Electric Propulsion Conference
University of Vienna • Vienna, Austria
September 15-20, 2019

Shinatora Cho[1]
Japan Aerospace Exploration Agency, Sagamihara, Kanagawa, 252-5210, Japan

Kentaro Hara[2]
Stanford University, Stanford CA, 94301

Hiroki Watanabe[3]
Tokyo Metropolitan University, Hino, Tokyo, 191-0065, Japan

Kenichi Kubota[4]
Japan Aerospace Exploration Agency, Chofu, Tokyo, 182-8522, Japan

and

Yusuke Yamashita
University of Tokyo, Hongo, Tokyo, Japan

Abstract: Radial-axial 2D3V fully kinetic particle simulation is conducted for a 100-W class Hall thruster. Singly, doubly, and triply charged ions are included and real particle mass and real electric permittivity are used. 100 ns steady state result shows the electron current is approximately 11% of the discharge current. The electron cross-field transport observed in particle simulation is compared to the fluid-based drift-diffusion framework. The results suggest the electron transport outside the channel is greater than the classical one by orders of magnitude; and electron inertia terms plays significant role there.

Nomenclature

B = magnetic field
E = electric field
e = unit charge
I_{inj} = electron injection current
k = Boltzmann constant
L_c = channel length

[1] Researcher, Research and Development Directorate, choh.shinatora@jaxa.jp.
[2] Assistant Professor, Aeronautics and Astronautics, kenhara@stanford.edu.
[3] Assistant Professor, Department of Aeronautics and Astronautics, hwatanabe@tmu.ac.jp.
[4] Researcher, Aeronautical Technology Directorate, kubota.kenichi@jaxa.jp.

h = channel width
m = electron mass
n = electron number density
r = radial position
S = Area
T_e = electron temperature
u = electron speed
z = axial position
ε = electric permittivity
μ = electron mobility
ν = electron momentum transfer collision frequency
ρ = charge density
Ω_e = electron Hall parameter

I.Introduction

Hall thrusters are efficient and robust electric propulsion which have been successfully applied to spacecraft maneuver for several decades. Recently, Hall thrusters are drawing more interests for wider range of applications such as all-electric satellites and micro-spacecraft. However, some aspects of Hall thruster's plasma discharge are not fully understood, such as the cross-field electron transport. The electron mobility across the magnetic field observed in Hall thruster plasmas is greater than the classical diffusion values by orders of magnitude, which suggests strong turbulent transport takes place. In this study, cross-field electron transport is investigated using a r-z two-dimensional particle-in-cell (PIC) Monte Carlo collision (MCC) simulation framework[1] in a 100-W thruster developed in Tokyo Metropolitan University.[2] The advantage of this simulation framework is that the plasma ionization, acceleration, and dissipation on walls are computed self-consistently, so that the energy conservation of the system is fulfilled. Various physics aspects, such as electron inertia, finite electron Larmor radius, and finite ion flow velocity, are also included, which is considered to be important for the instability growth and damping.[3] Electron cross-field transport is analyzed by comparing PIC results and electron mobility calculated using drift-diffusion framework. The importance of electron inertia terms, which are tend to be neglected without careful consideration, is discussed

II.Numerical Methods

JHAST f/p, an axial-radial two-dimensional fully kinetic Particle-In-Cell code is used in this study. Detail of the simulation framework can be found in previous studies.[4, 5] Table 1 summarizes the simulation setup. No artificial mass ratio, or permittivity acceleration techniques were used.[6] Timestep is small enough than the electron gyrofrequency and plasma frequency. Grid spacing is the Debye length assuming the electron number density ~ 5.0×10^{17} $[1/m^3]$ and electron temperature ~ 20 [eV]. The macro particle size is 2.5×10^5 real particles per simulation particle, which resulting approximately 150 simulation particles per cell in average for electron. Four kinds of particle species are computed including doubly and triply charged ions. Elastic and inelastic collisions including charge exchange collisions and coulomb collisions are implemented in a Monte-Carlo-Collision (MCC) manner. No anomalous collision models or additional transport models are used.

The governing equations is equation of motion (Eq. 1) for particles, and Poisson equation (Eq. 2) for electric fields. Both equations are discretized in cylindrical coordinates. Particle push is implemented by Runge-Kutta 4th order method and is coupled with field updates in a PIC framework. Semi-implicit source term is introduced to the discretized Poisson equation to stabilize the simulation.

$$m\dot{\boldsymbol{u}} = q(\boldsymbol{E} + \boldsymbol{u} \times \boldsymbol{B}) \tag{1}$$

$$\varepsilon \Delta \Phi = \rho \tag{2}$$

where, u is electron velocity, E is electric field, B is magnetic field. Table 2 tabulates the thruster specifications. The geometry of the thruster is targeted for 100-W operation having channel mean diameter of 20 mm. Figure 1 shows the computational domain and mesh. The axial length of the domain is taken 1.5 times the channel length. Electrons influx to the domain are implemented at both axial and radial plume boundaries in a quasi-neutral manner:

$$I_{inj} = e\rho u_{th} S \tag{3}$$

where, e is unit charge, ρ is the local charge density, u_{th} is electron thermal speed, and S is the area of the boundary. Note I_{inj} is set to zero if ρ is negative. The initial energy of injected electrons is set to 2 eV. This quasi-neutral electron injection method is important to avoid artificial effects caused by the boundary-induced charge imbalance.[5] The discharge voltage is 225V, and 200V was applied at the anode boundary, assuming the plasma-to-cathode potential is 25V.

Simulation was MPI parallelized and conducted on a 36 processors workstation. Approximately one-month of wall-clock time was necessary to finish 10-micro second computation.

Table 1. Simulation setup.

Timestep	1.0×10^{-12} s
Grid spacing	5.0×10^{-5} m
Mass ratio	*REAL*
Permittivity	*REAL*
Macro particle size	2.5×10^{5}
Particle species	e^-, Xe^+, Xe^{2+}, Xe^{3+}
Collision	$e^- - Xe$ elastic scattering $e^- - Xe$ excitation $e^- - Xe$ ionization $e^- - Xe^+$ ionization $e^- - Xe^{2+}$ ionization $Xe - Xe^+$ CEX $Xe - Xe^{2+}$ CEX $Xe - Xe^{3+}$ CEX Coulomb collisions
Anomalous collision models	*NONE*

Table 2. Thruster specifications.

Channel mean diameter	20 mm
Channel width	6 mm
Channel length	8 mm
Discharge voltage	225 V
Xe mass flow rate	0.5 mg/s
Magnetic field strength	20 mT at center of channel exit

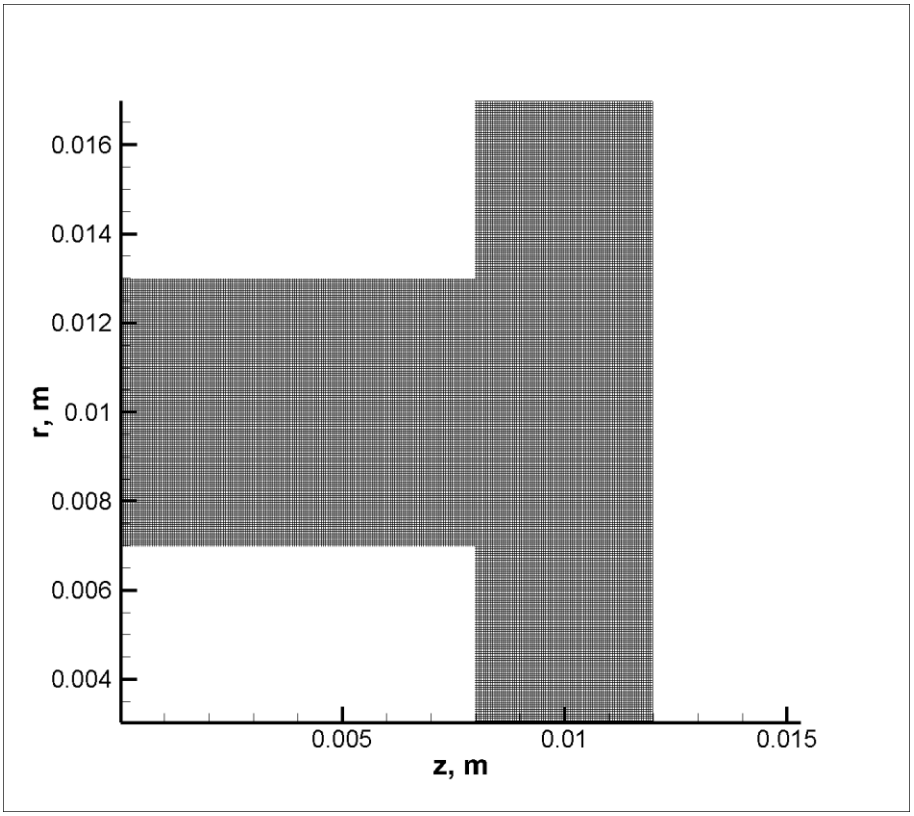

Figure 1. Computational domain and mesh.

III.Results and Discussion

A. Simulation results

Simulation was run until the discharge reaches a steady-state, and last 100 ns results were extracted with data sampling interval of 0.1 ns and presented in this study. Figure 2 presents the current results. Discharge current is net current collected on the anode. Note the ion current to the anode is negligibly small. Ion currents are collected on the plume boundaries for each charge state. Doubly charged ion current has roughly 11% contribution to the total ion current, whereas triply charged ion current is less than 2%. Electron current is calculated by subtracting ion current from discharge current, forming approximately 11% of discharge current. Although noise-like fluctuations exist, all current results are nearly constant over the 100 ns, suggesting the discharge is in a steady state.

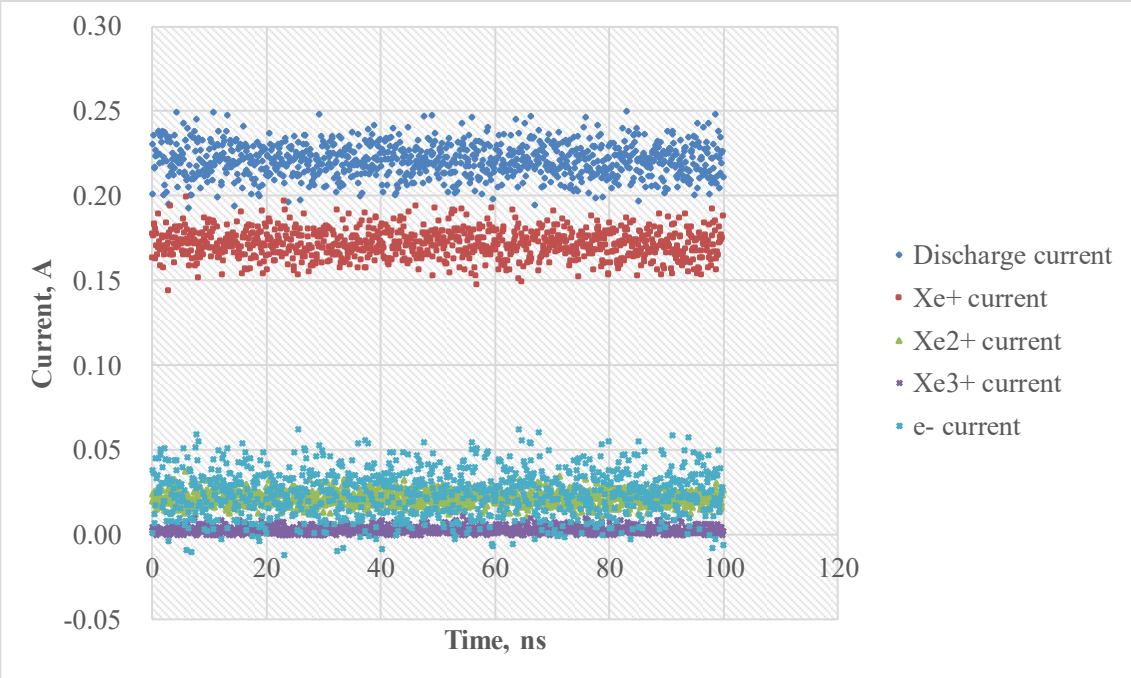

Figure 2. Simulation results of ion and electron currents.

Figure 3 displays simulation results of potential, electron temperature, electron number density, electron temperature, and ionization rate distributions. The results are time-averaged over 100 ns, the same time interval as figure 2, with sampling rate of 0.2 ns. The potential drop is focused on the area near channel exit, creating high density, high temperature, and high ionization rate region there. The radial peak of number density and ionization rate is shifted slightly outward from the channel centerline, suggesting the ion and electron current are mainly passing through the outer-half of the discharge channel.

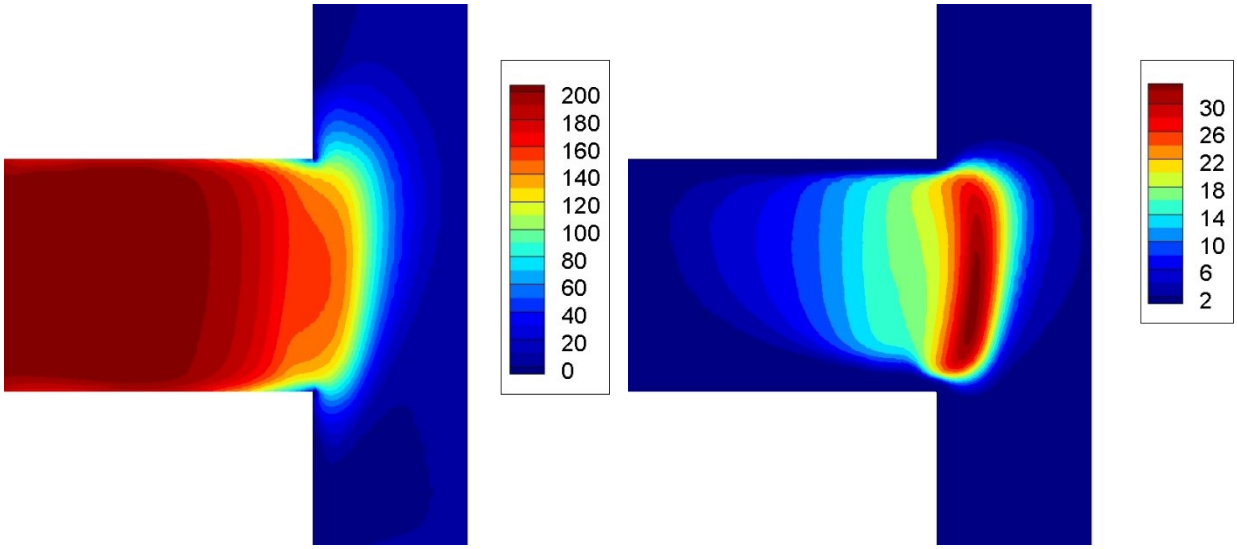

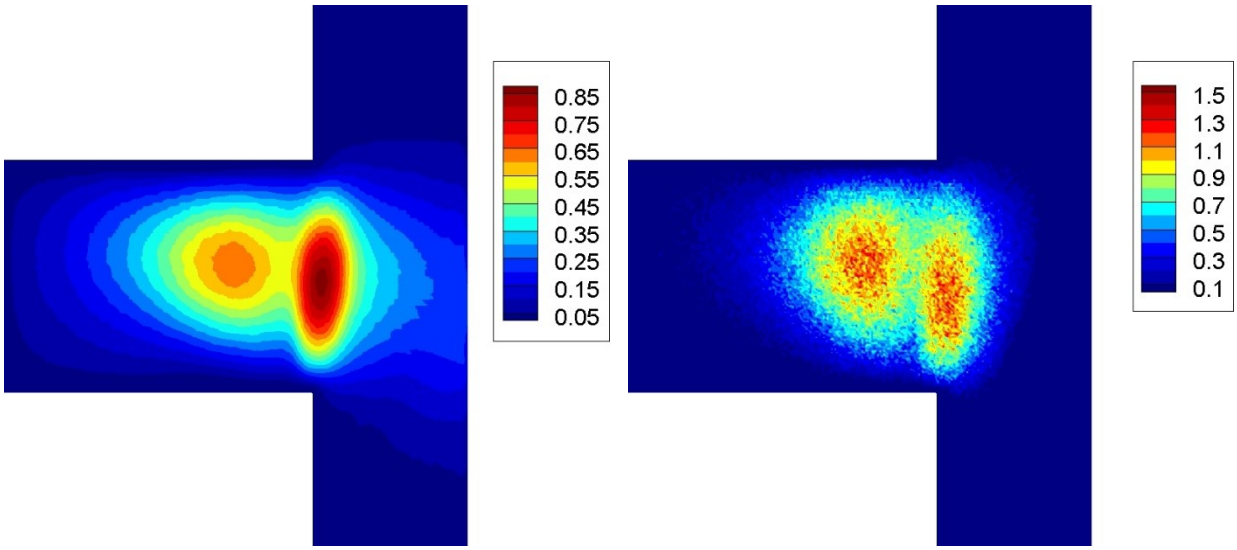

Figure 3. Simulation results of plasma properties. (left top) Potential[V], (left bottom) Electron number density[10^{18}/m^3], (right top) Electron temperature[eV], (right bottom) Ionization rate[10^{24}/(m^3 s)].

B. Discussion

The PIC simulation result is evaluated in a drift-diffusion framework to analysis the mechanism of derived electron transport. Electron drift-diffusion equation in a cylindrical coordinate write:

$$mn\left(\frac{\partial u_r}{\partial t}+u_r\frac{\partial u_r}{\partial r}+\frac{u_\theta}{r}\frac{\partial u_r}{\partial \theta}+u_z\frac{\partial u_r}{\partial z}-\frac{{u_\theta}^2}{r}\right)=-en(E_r+u_\theta B_z-u_z B_\theta)-\frac{\partial nkT_e}{\partial r}-mnvu_r \quad (4)$$

$$mn\left(\frac{\partial u_\theta}{\partial t}+u_r\frac{\partial u_\theta}{\partial r}+\frac{u_\theta}{r}\frac{\partial u_\theta}{\partial \theta}+u_z\frac{\partial u_\theta}{\partial z}+\frac{u_r u_\theta}{r}\right)=-en(E_\theta+u_z B_r-u_r B_z)-\frac{1}{r}\frac{\partial nkT_e}{\partial \theta}-mnvu_\theta \quad (5)$$

$$mn\left(\frac{\partial u_z}{\partial t}+u_r\frac{\partial u_z}{\partial r}+\frac{u_\theta}{r}\frac{\partial u_z}{\partial \theta}+u_z\frac{\partial u_z}{\partial z}\right)=-en(E_z+u_r B_\theta-u_\theta B_r)-\frac{\partial nkT_e}{\partial z}-mnvu_z \quad (6)$$

where, m is electron mass, n is electron number density, T_e is electron temperature, and ν is momentum transfer collision frequency. Ignoring E_θ, $\partial/\partial\theta$, B_z, and electron inertia terms on the left-hand side, classical electron mobility $\mu_\perp$ can be derived as:

$$0=-enu_z B_r-mnvu_\theta \quad (7)$$

$$0=-en(E_z-u_\theta B_r)-\frac{\partial nkT_e}{\partial z}-mnvu_z \quad (8)$$

$$u_z=\frac{\frac{-e}{mv}}{1+\left(\frac{eB_r}{mv}\right)^2}\left(E_z+\frac{1}{en}\frac{\partial nkT_e}{\partial z}\right)=\mu_\perp\left(E_z+\frac{1}{en}\frac{\partial nkT_e}{\partial z}\right)\equiv u_{z_{classical}} \quad (9)$$

However, it is questionable if the inertia terms are truly negligible because typical electron ExB drift velocity u_θ in Hall thrusters is as large as 10^6 m/s. If u_θ inertia terms are left, equations become:

$$mn\left(-\frac{{u_\theta}^2}{r}\right)=-enE_r-\frac{\partial nkT_e}{\partial r}-mnvu_r \quad (10)$$

$$mn\left(u_r\frac{\partial u_\theta}{\partial r}+u_z\frac{\partial u_\theta}{\partial z}+\frac{u_r u_\theta}{r}\right)=-enu_z B_r-mnvu_\theta \quad (11)$$

$$0 = -en(E_z - u_\theta B_r) - \frac{\partial nkT_e}{\partial z} - mn\nu u_z \tag{12}$$

where Eq. 10 shows the balance between the centrifugal force, radial electric field, pressure, and drag. From Eq. 11 and 12, the effect of inertia terms can be written as the analogy of Reynolds stress in Navier–Stokes equations:

$$u_z = \frac{\frac{-e}{m\nu}}{1+{\Omega_e}^2}\left\{E_z + \frac{1}{en}\frac{\partial nkT_e}{\partial z} + \frac{B_r}{\nu}\left(\overline{u_r\frac{\partial u_\theta}{\partial r}} + \overline{u_z\frac{\partial u_\theta}{\partial z}} + \frac{\overline{u_r u_\theta}}{r}\right)\right\} \tag{13}$$

$$\Omega_e = \frac{eB_r}{m\nu} \tag{14}$$

where the bar denotes the variable is a time-averaged value. Very simple order estimation could show the importance of these terms, for example at ion acceleration region, $\overline{\partial u_\theta/\partial z} \sim 10^9, \overline{u_z} \sim 10^4, \nu \sim 10^6$, thus the mean value of

$$\frac{B_r}{\nu}\cdot\overline{u_z}\cdot\overline{\frac{\partial u_\theta}{\partial z}} \sim 10^5 \tag{14}$$

is on the same order of magnitude as E_z. Moreover, the Reynolds stress R could make this term even greater as:

$$\overline{u_z\frac{\partial u_\theta}{\partial z}} = \overline{u_z}\cdot\overline{\frac{\partial u_\theta}{\partial z}} + R \tag{15}$$

It is notable that the effective electron mobility could be negative depending on the sign and magnitude of the inertia terms. Using the PIC simulation result, the importance of the inertia terms is evaluated by comparing the actual u_z in the PIC simulation (u_{z_PIC}) and the one calculated from drift-diffusion equations (u_{z_dd}) as:

$$u_{z\_dd} = u_{z\_classical} + u_{z\_inertia} \tag{16}$$

where, $u_{z\_inertia}$ is the contribution of inertia terms in the $\Omega_e \gg 1$ limit.

$$u_{z\_inertia} = -\frac{m}{eB_r}\left(\overline{u_r\frac{\partial u_\theta}{\partial r}} + \overline{u_z\frac{\partial u_\theta}{\partial z}} + \frac{\overline{u_r u_\theta}}{r}\right) \tag{17}$$

Figure 4 shows the result on the channel centerline, and centerline ∓2 mm. u_{z_PIC} is the result of PIC simulation, u_{z_dd} is calculated using Eq. 16, and $u_{z_{classical}}$ is calculated using Eq. 9. X-axis is the axial position normalized by channel length where z/Lc=1 is the channel exit. Minus velocity means the electron current is heading toward the anode. u_{z_PIC} deviates from $u_{z_{classical}}$ by several orders of magnitude in the z/Lc>1.2 plume region, suggesting significant so-called anomalous electron transport exists there. It is noteworthy that on the channel centerline, u_{z_PIC} is partially directed against the anode despite the axial electric field is positive, suggesting negative electron mobility region exists. On the other hand, u_{z_PIC} is greatly negative on channel centerline +2mm, so the electron current seems to be passing through the outer-half of the channel toward the anode. u_{z_dd} agrees with these trends at least on the order of magnitude, that similar enhanced and negative electron mobility can be found in plume region. These results indicate that the plume region electron mobility observed in PIC simulation is largely governed by the electron inertia terms in drift-diffusion framework, rather than the electric field and pressure diffusion. However, the matching of u_{z_PIC} and u_{z_dd} is not perfect quantitatively in the plume region. The reason of this discrepancy can be attribute to the effects of B_z, or other inertia terms we dropped from Eq. 10-12. Moreover, kinetic effects can also play important role such as finite Larmor radius and non-Maxwellian velocity distribution. The derivations of the fluid equations taking the moments from the kinetic equations are discussed in IEPC-2019-691.[7] In the inside channel region, the influence of electron inertia terms is limited that u_{z_dd} agrees well with $u_{z_{classical}}$, which is because of the collisionality. The deviation of u_{z_PIC} from $u_{z_{classical}}$ inside the channel is likely to be attributed to other mechanisms such as wall effects.

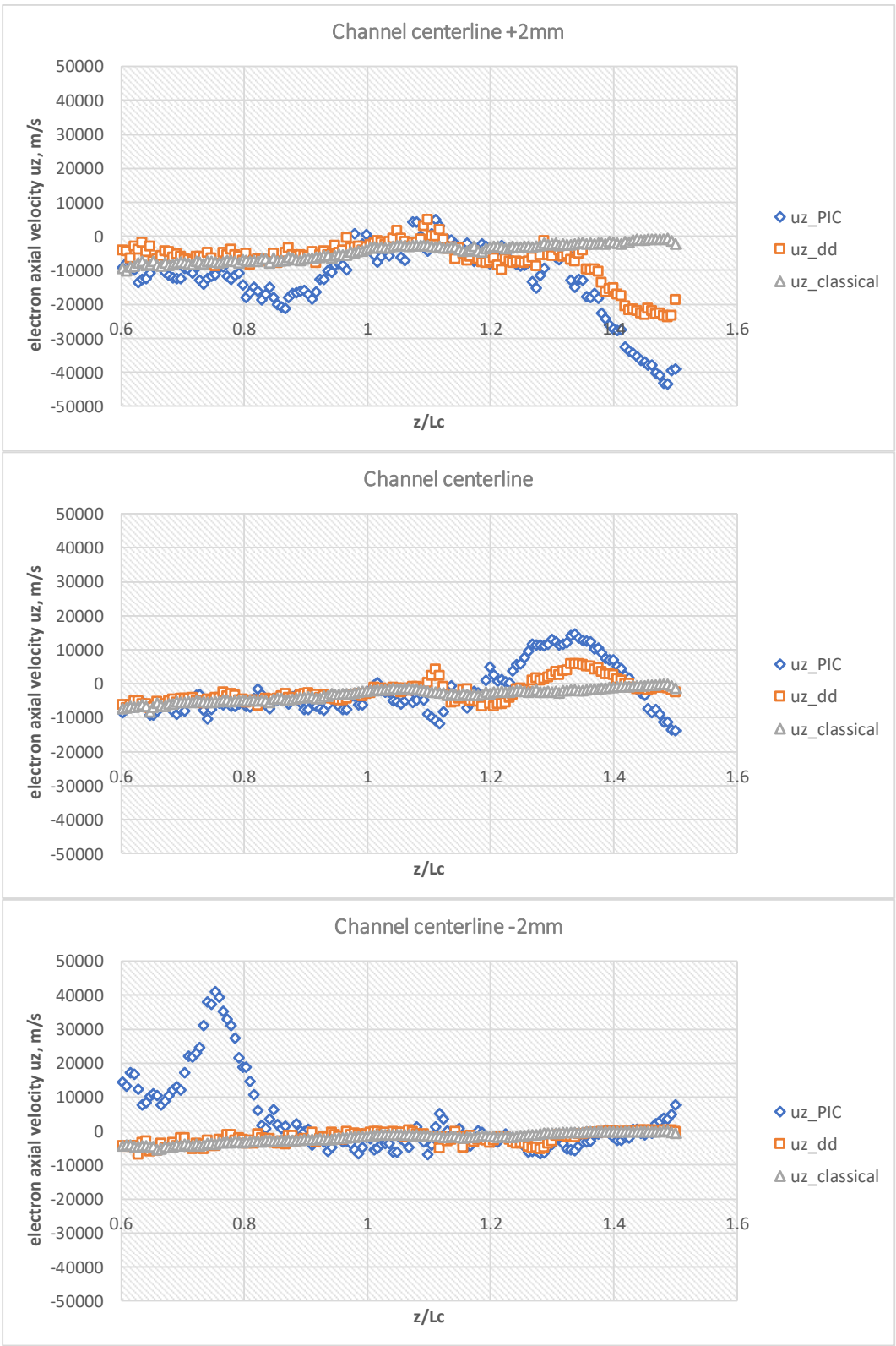

Figure 4. Comparison of electron axial velocity. u_{z_PIC} is the result of PIC simulation, u_{z_dd} is calculated using drift-diffusion equation, and $u_{z\_classical}$ is calculated using Eq. 9. X-axis is the axial position normalized by channel length where z/Lc=1 is the channel exit. Minus velocity means the electron current is heading toward the anode.

IV.Conclusion

A radial-axial 2D3V fully kinetic particle simulation result on a 100-W class Hall thruster is reported. Real mass, real permittivity steady-state result suggests the importance of electron inertia terms on electron cross-field transport outside the discharge channel.

Acknowledgments

This work was supported by JSPS KAKENHI Grant Numbers JP18K13932, JP18H03815.

References

[1]S. Cho, et al Phys. Plasmas 20, 063501 (2013).
[2]H. Watanabe, S. Cho, K. Kubota, IEPC-2019-447.
[3]N A Marusov et al 2019 Plasma Sources Sci. Technol. 28 015002.
[4]Cho S, Watanabe H, Kubota K, Iihara S, Fuchigami K, Uematsu K and Funaki I 2015 Phys. Plasmas 22 103523
[5]Cho S., Watanabe H, Kubota K, Hara, K., IEPC-2017-402
[6]Boeuf J. P., J. Appl. Phys. 121, 011101 (2017);
[7]Hara, K., Yamashita, Y., Tsikata S., Vincent B., Mazouffre S., Cho S., IEPC-2019-691